Half-lives and cluster preformation factors for various cluster emissions in trans-lead nuclei

Dongdong Ni[1,2,*] and Zhongzhou Ren[1,2,3,†]
[1]*Department of Physics, Nanjing University, Nanjing 210093, China*
[2]*Kavli Institute for Theoretical Physics China, Beijing 100190, China*
[3]*Center of Theoretical Nuclear Physics, National Laboratory of Heavy-Ion Accelerator, Lanzhou 730000, China*
(Received 1 July 2010; published 12 August 2010)

The generalized density-dependent cluster model (GDDCM) is extended to study cluster radioactivity in even-even and odd-A nuclei decaying to the doubly magic nucleus ^{208}Pb or its neighboring nuclei. The microscopic cluster-daughter potential is numerically constructed in the double-folding model with M3Y nucleon-nucleon interactions plus proton-proton Coulomb interactions. Instead of the WKB barrier penetration probability, the exact solution of the Schrödinger equation with outgoing Coulomb wave boundary conditions is presented. The cluster preformation factor is well taken into account based on some available experimental cases. The calculated half-lives are found to be in good agreement with the experimental data. This indicates that a unified description of α decay and cluster radioactivity has been achieved by the GDDCM. Predictions of cluster emission half-lives are made for promising emitters, which may guide future experiments.

DOI: 10.1103/PhysRevC.82.024311 PACS number(s): 23.70.+j, 21.10.Tg, 21.60.Gx, 27.90.+b

I. INTRODUCTION

The spontaneous emission of a charged particle heavier than an α particle but lighter than the lightest fission fragment is known as cluster radioactivity. This new radioactivity decay mode was first predicted in 1980 by Săndulescu, Poenaru, and Greiner [1]. Subsequently in 1984 Rose and Jones experimentally observed this new kind of radioactivity, ^{14}C emission from ^{223}Ra [2]. The whole family of such a disintegration mode consists of carbon radioactivity, oxygen radioactivity, neon radioactivity, magnesium radioactivity, silicon radioactivity, and so on. The parent nuclei range from ^{221}Fr to ^{242}Cm, decaying to the doubly magic nucleus ^{208}Pb or its neighboring nuclei. It is evident that this new radioactivity is closely related to the extra stability of the daughter nuclei. In order to understand this new radioactivity which occupies an intermediate position between α decay and nuclear fission, many explicit quantitative studies have been carried out from two standpoints. One is the adiabatic treatment based on the fissionlike theory [1,3–8], where the decay process is described by a continuous change of geometrical shapes and the cluster is considered to be formed gradually during the adiabatic rearrangements of parent nuclei. The superasymmetric fission model (SAFM) [3,4], which has contributed significantly to the knowledge of nuclear hadronic decays, belongs to this category. The other is the nonadiabatic treatment based on the traditional α-decay approach [9–16], where the cluster is treated to be preformed in the decaying nucleus with a certain preformation probability.

The renewed interest in cluster radioactivity has recently been stimulated partly by the unified description of various hadronic decays, and partly by the very recent experiments on the cluster radioactivity of ^{238}U by ^{34}Si emission and the one of ^{223}Ac by ^{14}C and ^{15}N emissions [17,18]. The density-dependent cluster model (DDCM), combined with the simple assumption of the cluster preformation factor, has been employed to calculate half-lives of cluster radioactivity for various clusters, and the results show good agreement with the available experimental data [13]. Within the generalized liquid-drop model (GLDM), the cluster preformation factor P_c is extracted by dividing the experimental decay width by the product of the Wentzel-Kramers-Brillouin (WKB) penetration probability and the assault frequency, and the extracted P_c values agree well with the previous studies [16]. The preformed cluster model (PCM) has recently been improved by taking into account the deformations and orientations of nuclei [12]. Within the Coulomb and proximity potential model (CPPM), the cluster formation probability is calculated as the penetrability probability through the internal part of the potential barrier, and it is concluded that the emission of α-like clusters is preferred for trans-tin nuclei while the emission of non-α-like clusters is preferred for trans-lead nuclei [8]. We also notice that there are several investigations focused on a unified analytical formula of half-lives for α decay and cluster radioactivity [19–22]. All of these studies should be considered as effective methods to give precise descriptions of cluster radioactivity, since they are based on different models or different variations of Gamow's theory. In addition, we would like to point out that in recent studies Poenaru *et al.* have performed a detailed study of the singly ionized trimer emission from charged metallic atomic clusters by extending the fission and α-decay theory to nanophysics [23,24]. This is of great interest and worth further investigation.

Very recently we have proposed the generalized density-dependent cluster model (GDDCM) for α decay [25–27]. Within this model, α-decay half-lives are evaluated from the quasibound solution of the Schrödinger equation, and the good agreement between experiment and theory is achieved for a wide range of nuclei, including exotic α emitters around the significant $N = 126$ shell gap and α-decaying isomers [25,26]. In view of the fact that α decay and cluster radioactivity are

*dongdongnick@gmail.com
†zren@nju.edu.cn

physically similar processes, both being quantum tunneling through the potential barrier [28–30], we hope to achieve a unified description of them. As a further extension of the GDDCM toward cluster radioactivity, the present study reports on a detailed study of cluster radioactivity within the GDDCM framework.

This article is organized in the following way. In Sec. II we present the theoretical framework of the GDDCM and the phenomenological analysis of the cluster preformation factor. In Sec. III the cluster-daughter potential and quasi-bound-state wave function are discussed in detail, together with the model parameters used in the calculations. The theoretical results of our calculations are compared with the experimental data, and some predictions of cluster emission half-lives are made for possible candidates. A summary is given in Sec. IV.

II. THEORETICAL FRAMEWORK OF THE GENERALIZED DENSITY-DEPENDENT CLUSTER MODEL

The absolute calculation of cluster radioactivity consists of two aspects. The nuclear structure part of the problem is associated with the extent to which the cluster is preformed in the decaying nucleus. This can be taken into account by introducing the cluster preformation factor P_c. The nuclear reaction part of the problem concerns the penetration of the preformed cluster through the potential barrier. This has been widely investigated in terms of the quantum tunneling effect. In the cluster representation of the decaying nucleus, we proceed by constructing microscopic Coulomb and nuclear potentials, and solving the stationary Schrödinger equation that describes the relative motion of the cluster with respect to the core nucleus,

$$\left(-\frac{\hbar^2}{2\mu}\frac{d^2}{dr^2} - V(r)\right) u_{n\ell j}(r) = Q u_{n\ell j}(r). \tag{1}$$

The interaction potential $V(r)$ includes the repulsive Coulomb part, the attractive nuclear part, and the additional centrifugal part,

$$V(r) = V_C(r) + V_N(r) + \frac{\ell(\ell+1)\hbar^2}{2\mu r^2}, \tag{2}$$

where μ is the reduced mass of the system, and ℓ is the angular momentum carried by the cluster. The nuclear potential is obtained using the double-folding method with effective nucleon-nucleon (NN) interactions. The Coulomb potential is also obtained in the double-folding model where the matter-density distributions of nuclei are replaced by their charge density distributions. They are written in the following form [31–33]:

$$V_{N\,\mathrm{or}\,C}(\mathbf{r}) = \lambda \int d\mathbf{r_1} d\mathbf{r_2} \rho_1(\mathbf{r_1}) \upsilon(\mathbf{s}) \rho_2(\mathbf{r_2}), \tag{3}$$

where the factor λ is employed to renormalize the nuclear potential to reproduce an equivalent local potential ($\lambda = 1$ for the Coulomb potential), and $\upsilon(\mathbf{s} = |\mathbf{r} + \mathbf{r_2} - \mathbf{r_1}|)$ is the effective NN interaction or the standard proton-proton Coulomb interaction. The density distributions of the cluster and the residual core nucleus have the well-known two-parameter Woods-Saxon form,

$$\rho_{1,2}(r) = \frac{\rho_0}{1 + \exp\left[(r - R)/a\right]}, \tag{4}$$

where ρ_0 is determined by integrating the density distribution equivalent to the mass number A (or atomic number Z) of corresponding nuclei. The radius parameter R is taken to be $R = 1.07A^{1/3}$, and the diffuseness a is fixed at $a = 0.54$ [34,35]. It should be noted that if the cluster is an α particle, its density distribution is described by the standard Gaussian form [27,33]. For the effective NN interaction, we use the popular Michigan three-range Yukawa (M3Y)–Reid-type interaction, which is one of the most widely used interactions. Its parametrized form, introduced by Satchler and Love [36], is written as

$$\upsilon(\mathbf{s}) = 7999\frac{\exp(-4s)}{4s} - 2134\frac{\exp(-2.5s)}{2.5s} + J_{00}(E_c)\delta(\mathbf{s}), \tag{5}$$

and the zero-range pseudopotential $J_{00}(E_c)$ representing the single-nucleon exchange effect is given by

$$J_{00}(E_c) = -276[1 - (0.005E_c/A_c)], \tag{6}$$

where E_c and A_c are the kinetic energy and mass number of the cluster, respectively.

With this microscopic cluster-daughter potential, the Schrödinger equation (1) is numerically solved for the quasi-bound-state wave function $u_{n\ell j}(r)$. Since the decay energy Q cannot be predicted with sufficient accuracy, following the procedure of α-decay calculations [25–27], we adjust the renormalized factor λ of the nuclear potential to reproduce the decay Q value. Then, we consider the Pauli exclusion principle for the nucleons in the preformed cluster with respect to those in the core nucleus, which would result in a nonlocal cluster-core interaction. On the one hand, the single-nucleon exchange term has been included in the effective M3Y–Reid-type interaction, as shown by Eq. (5). On the other hand, the quantum number n (i.e., the number of internal nodes in the radial wave function) is chosen to satisfy the Wildermuth rule [37], which relates the quantum numbers of the cluster to the shell-model quantum numbers of the nucleons forming the cluster in the following way:

$$G = 2n + \ell = \sum_{i=1}^{A_c} \left(g_i^{(A_d+A_c)} - g_i^{(A_c)}\right). \tag{7}$$

In this expression, $g_i^{(A_d+A_c)}$ are the oscillator quantum numbers of the nucleons forming the cluster, whose values are required to ensure the cluster completely outside the shell occupied by the core nucleus, and $g_i^{(A_c)}$ are the internal quantum numbers of the A_c nucleons in the shell model of the cluster. Here, we take $g_i = 4$ for nucleons in the $50 \leqslant Z, N \leqslant 82$ shell, $g_i = 5$ for nucleons in the $82 < Z, N \leqslant 126$ shell, and $g_i = 6$ for nucleons outside the $N = 126$ neutron shell closure. This rule is sufficient to account for the main effects of the Pauli principle, and the remaining effects are mostly absorbed into the effective cluster-daughter potential based on the popular M3Y–Reid-type interaction.

Next, for the Coulomb-nuclear problem, the quasibound solution $u_{n\ell j}(r)$ of Eq. (1) is obtained by matching it to a purely outgoing Coulomb wave in the asymptotic region [27],

$$u_{n\ell j}(r) \to G_\ell(kr) + i\,F_\ell(kr), \tag{8}$$

where $G_\ell(kr)$ and $F_\ell(kr)$ are, respectively, the irregular and regular Coulomb wave functions with $k = \sqrt{2\mu Q}/\hbar$. After this, the overall normalization of $u_{n\ell j}(r)$ is achieved by requiring that

$$\int_0^{R_{\max}} |u_{n\ell j}(r)|^2 dr = 1. \tag{9}$$

Here the cutoff radius $R_{\max}$ is fixed at $R = 30$ fm, but any radius in the exterior region yields the approximately same normalization. This is because the wave function $u_{n\ell j}(r)$ decreases rapidly with a radius outside the nucleus.

The decay width is determined from the decay probability current through a spherical surface, which is calculated with the asymptotical behavior of the radial wave function, $u_{n\ell j}(r) \simeq N_{\ell j}[G_\ell(kr) + i\,F_\ell(kr)]$. Ultimately, one can give an expression for the width of the form [27]

$$\Gamma = \frac{\hbar^2 k}{\mu}|N_{\ell j}|^2, \tag{10}$$

where the constant $N_{\ell j}$ can be expressed as the ratio of the quasi-bound-state wave function $u_{n\ell j}(r)$ to the outgoing Coulomb wave at a large distance R. Then, the decay width representing the tunneling through the potential barrier is given by [27]

$$\Gamma(R) = \frac{\hbar^2 k}{\mu}\frac{|u_{n\ell j}(R)|^2}{G_\ell(kR)^2 + F_\ell(kR)^2}. \tag{11}$$

It is particularly worth noting that the expression of Eq. (11) is valid only for distances beyond the range of the nuclear potential and shows rather weak sensitivity to the choices of R. This property can provide a convenient self-check of the reliability of the exact formalism presented here.

To calculate absolute cluster emission half-lives, it is indispensable to include the cluster preformation factor P_c, which measures the extent to which the cluster is preformed at the nuclear surface. It is well known that the cluster formation is one of the basic features in nuclear many-body dynamics, and cluster structure is very important in light nuclei [38]. For the clustering in heavy nuclei, it is known from available experimental cases that the factor P_c usually differs widely from one decay mode to another but varies very slowly for a given radioactivity. More precisely, the factor P_c decreases considerably in magnitude with increasing the size of the cluster [39]. With this in mind, the preformation factor of a cluster depends practically upon the size of the cluster. Besides this, in view of the fact that the same cluster is emitted by different nuclei, the preformation factor should essentially associate with the size of the parent nucleus or its daughter. Based on these simple experimental facts, we assume that the cluster preformation factor P_c has an exponential form as follows [21]:

$$P_c = 10^{-a\sqrt{\mu}(Z_c Z_d)^{1/2}+b}, \tag{12}$$

where the reduced mass μ is measured in unit of the nucleon mass, $\mu = A_c A_d/(A_c + A_d)$, Z_c and Z_d are, respectively, the atomic numbers of the cluster and the daughter nucleus, and a and b are free parameters to be determined. Within this expression, for a given cluster, taking an α particle, for example, the quantities $\sqrt{\mu}$ and $(Z_c Z_d)^{1/2}$ change very smoothly with parent nuclei in the heavy and superheavy mass region so that the preformation factor is almost constant for α decay. This is quite consistent with the available experimental results [40]. Moreover, through the physical quantities μ and Z_c, as expected, the factor P_c in Eq. (12) exhibits a strong decrease in magnitude with an increase in the size of the cluster. Before ending the analysis of the factor P_c, we would like to point out that there are other ways to evaluate the cluster preformation factor P_c. The clear dependence of P_c upon the mass number of emitted clusters was found for various clusters with mass number up to $A_c = 28$ [41], which is given by

$$P_c = [P_\alpha]^{(A_c-1)/3}, \tag{13}$$

where P_α is the preformation factor of an α particle with different values for even-even and odd-A parent nuclei. In Refs. [9,12,14], the cluster preformation factor is defined as the probability of finding two fragments (the cluster and the daughter nucleus) at a fixed relative separation R, and its evaluation is achieved by solving the stationary Schrödinger equation for the dynamical flow of mass and charge. Within the fissionlike model [6,8], the cluster preformation probability is calculated as the penetrability probability through the internal part of the potential barrier.

III. NUMERICAL RESULTS AND DISCUSSIONS

A. Double-folding potential and quasi-bound-state wave function

In the cluster model of the decaying nucleus, reliable input of the cluster-nucleus interaction potential is essential for the quantitative description of α decay or cluster radioactivity. In contrast to the WKB penetration probability only connected with the potential barrier, the present GDDCM calculation, based on the quasi-bound-state wave function, has a clear dependence upon the entire potential. Hence, the double-folding potential is strikingly appropriate and rewarding to our approach owing to its microscopic nature. It is interesting to gain deep insight into the microscopic potential presented here. Figure 1(a) shows the microscopic double-folding potential of the ^{208}Pb + ^{14}C system in three different kinds: nuclear, Coulomb, and total potentials. For the sake of convenience, we also give the microscopic potential of the ^{208}Pb + α system in Fig. 1(b). With respect to the ^{208}Pb + α system, the ^{208}Pb + ^{14}C system has a significantly deeper nuclear potential well and a much higher Coulomb potential barrier in the interior region. Obviously, the heavier the cluster, the larger the finite depth of total potentials.

It is also interesting to look in detail at the systematic behavior of the quasi-bound-state wave function $u_{n\ell j}(r)$. Figure 2 illustrates the interior and exterior properties of the real part of the wave function $u_{n\ell j}(r)$ for the ^{208}Pb + ^{14}C system. We would like to point out that the y axis in Fig. 2(b)

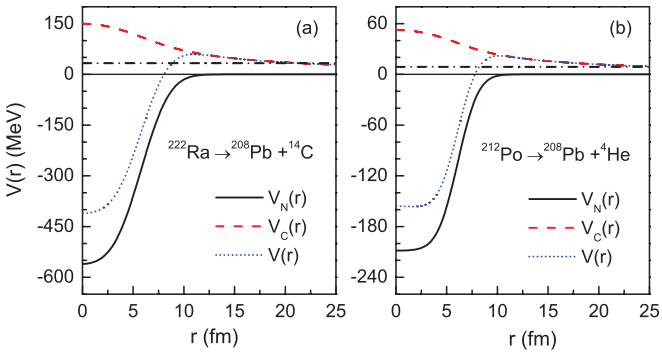

FIG. 1. (Color online) Schematic sketch of the double-folding nuclear potential $V_N(r)$ (the black solid line), the double-folding Coulomb potential $V_C(r)$ (the red dashed line), and the total potential $V(r) = V_N(r) + V_C(r)$ (the blue dotted line): (a) for the $^{208}\mathrm{Pb} + {}^{14}\mathrm{C}$ system and (b) for the $^{208}\mathrm{Pb} + \alpha$ system. The decay Q value is also indicated by the dashed-dotted line.

is magnified by 10^{14}, that is, the $u_{n\ell j}(r)$ real part decreases actually by about 14 orders of magnitude in the barrier region. Furthermore, this strong amplitude attenuation is more obvious for heavier clusters. In the exterior region, the real part of $u_{n\ell j}(r)$ does not seem to vanish completely like a bound-state wave function. Instead, it is characterized by the oscillatory behavior of the Coulomb wave, although its amplitude is vanishingly small. This is the most significant difference between quasi-bound-state wave functions and bound-state ones.

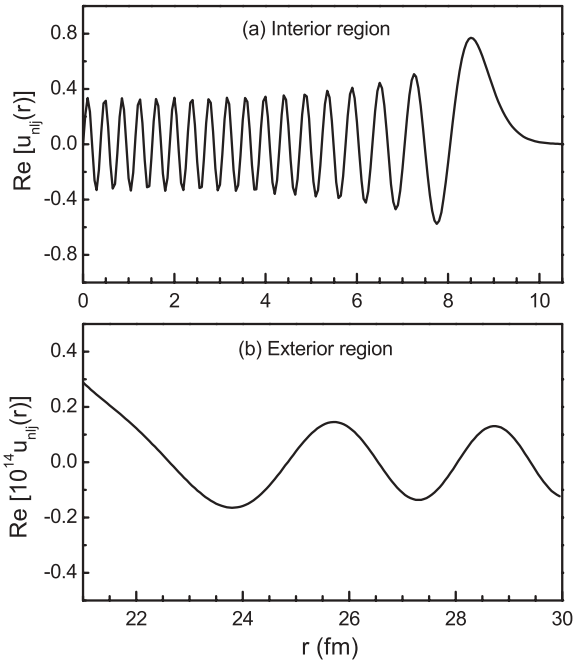

FIG. 2. The real part of the quasi-bound-state wave function $u_{n\ell j}(r)$ for the $^{208}\mathrm{Pb} + {}^{14}\mathrm{C}$ system: (a) in the interior region and (b) in the exterior region. It is worthwhile to note that the y axis in (b) is magnified by 10^{14}. This suggests that the wave function is damped by about 14 orders of magnitude in the barrier region.

B. Model parameters used in calculations

Within the GDDCM, the microscopic cluster-daughter potential is numerically constructed in the double-folding model using the density distributions of the cluster and the core nucleus, which are defined by the radius R and diffuseness a. The parametrization of R and a is taken from the classical nuclear textbooks [34,35]. In the course of solving the Schrödinger equation, the only adjustable parameter is the renormalized factor λ in the double-folding nuclear potential. Its value is determined from the eigencharacteristic of the cluster quasi-bound-state, such as the decay Q value and the quantum number n. In the whole calculation of various cluster emissions, the λ value is found to vary slowly in the range from 0.437 to 0.543.

As the last step to calculate cluster emission half-lives, the additional quantity, namely the cluster preformation factor P_c, is introduced into the calculation. As mentioned, the analysis of P_c can conveniently be made by the simple expression Eq. (12). Considering the unpaired nucleon in odd-A nuclei and the proton-neutron coupling in odd-odd nuclei, there exist different hindrance in even-even, odd-A, and odd-odd emitters. And these hindrance have a direct effect on the cluster preformation factor P_c. As a result, in the systematic study of all kinds of emitters, the parameter a in Eq. (12) remains the same for even-even, odd-A, and odd-odd nuclei, while the parameter b has three different values. In this way, the difference among various hindrance is taken into account in a straightforward and consistent manner. In our calculations, the experimental cluster preformation factor is defined as the ratio between the experimental and calculated decay widths,

$$P_c^{\mathrm{expt}} = \Gamma_{\mathrm{expt}}/\Gamma_{\mathrm{calc}}, \tag{14}$$

where the experimental decay width Γ_{expt} is related to the measured half-life $T_{1/2}$ by the well-known relationship $\Gamma_{\mathrm{expt}} = \hbar \ln 2/T_{1/2}$. Through a fitting procedure to the P_c^{expt} values, we find that the experimental P_c factors can be reproduced by the following parameters:

$$\begin{aligned} a &= -0.052, \\ b_{e-e} &= 0.690, \\ b_{o-A} &= -0.600. \end{aligned}$$

In terms of these parameters, the α-preformation factor for ^{212}Po has a value of 0.23. This agrees well with both the microscopic calculation of ^{212}Po [42] and the systematic calculation of α decay [27].

C. Systematic results of half-lives for α decay and cluster radioactivity

Using the formalism described above, we have performed a systematic investigation on cluster radioactivity in the trans-lead region. For comparison we also present an α-decay study of the α emitters decaying to the doubly nucleus ^{208}Pb or its neighboring nuclei. For ground-state-to-ground-state transitions, the decay Q value is calculated from the relationship

$$Q(Z, A) = B(Z_d, A_d) + B(Z_c, A_c) - B(Z, A), \tag{15}$$

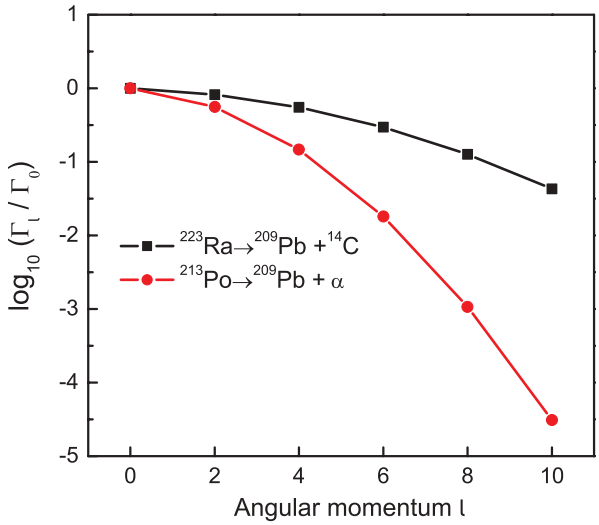

FIG. 3. (Color online) Sensitivity of the calculated decay width to the relative angular momentum ℓ for the ^{209}Pb + ^{14}C and ^{209}Pb + α systems. Calculations are performed at various assumed ℓ values within the GDDCM framework.

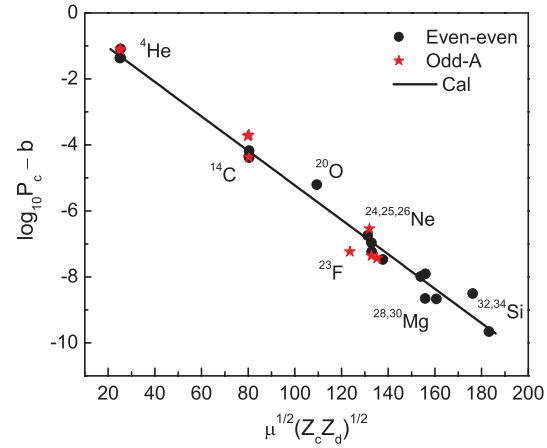

FIG. 4. (Color online) Comparison of the logarithms of the calculated cluster preformation factors and the experimental values for various clusters emitted from even-even and odd-A nuclei. The line represents the calculated values and the points stand for the experimental ones. The parameter b in the y axis has two different values for even-even and odd-A emitters, showing the well-known odd-even effect of mass number.

where the binding energies $B(Z_d,A_d)$,$B(Z_c,A_c)$, and $B(Z,A)$ are all taken from Ref. [43]. For even-even nuclei, the decay always ends up in even-even products. All ground states involved are characterized by the spin-parity of 0^+, and thus all the decays are favored transitions (i.e., $\ell = 0$). For odd-A nuclei, the decay proceeds from parent ground states to daughter ground states by emission of an even-even cluster or, occasionally, an odd-A cluster. The relative angular momentum ℓ cannot be unambiguously determined like that of even-even nuclei. In this case, we adopt the smallest one among all allowed ℓ values. This is a reasonable procedure because in most cases the cluster prefers to carry the smallest angular momentum. On the other hand, the centrifugal barrier plays a minor role in cluster radioactivity due to the large cluster-daughter reduced mass μ and also because the Coulomb potential becomes relatively large. For concreteness, in Fig. 3 we present the calculated decay width Γ_ℓ relative to the $\ell = 0$ case as the function of the ℓ value for the ^{14}C radioactivity of ^{223}Ra and the α decay of ^{213}Po. One can see that the calculated decay width decreases with increasing the ℓ value in both the α decay and the ^{14}C radioactivity. More importantly, as the ℓ value is changed from 0 to 8, the decay width for the ^{209}Pb + ^{14}C system decreases by almost one order of magnitude while the decay width for the ^{209}Pb + α system decreases by about three orders of magnitude. This clearly shows that there is a much weaker sensitivity of the calculated decay width to the ℓ value for the ^{14}C radioactivity of ^{223}Ra than for the α decay of ^{213}Po, especially in the high relative angular momentum region.

For a clear insight into the correlation between the preformation factors of various clusters, the $P_c^{\rm expt}$ values are illustrated in the logarithmic plot of Fig. 4 for both even-even and odd-A nuclei, together with the P_c values calculated with the analytical formula Eq. (12). The x axis of Fig. 4 denotes the exponential term $\sqrt{\mu}(Z_cZ_d)^{-1/2}$ and the y axis stands for the quantity $(\log_{10} P_c - b)$, where the well-known odd-even effect of the mass number is included by two different values of the parameter b. One can obviously see that the experimental points lie approximately in a single straight line as predicted by the formula Eq. (12). This makes an active response to our assumption of the cluster preformation factor and gives us confidence to make precise calculations of cluster emission half-lives.

Table I displays the detailed numerical results of the emissions of various clusters from even-even and odd-A nuclei, for which the experimental decay half-lives are available with reasonable accuracy. For comparison the unified formula of half-lives for α decay and cluster radioactivity is also applied to evaluate cluster emission half-lives, which is given by [21]

$$\log_{10} T_{1/2} = a\sqrt{\mu}Z_cZ_dQ^{-1/2} + b\sqrt{\mu}(Z_cZ_d)^{1/2} + c, \quad (16)$$

where the half-life $T_{1/2}$ is in seconds, and the Q value is in MeV. In Table I, the first column denotes the spontaneous emission of a cluster from parent nuclei. The second and third columns label the decay energy and the calculated cluster preformation factor, respectively. The experimental cluster emission half-lives are listed in the fourth column. The last two columns give the theoretical half-lives calculated with the GDDCM and with the unified formula, Eq. (16). It is known that the present data of many emitters have a large measuring error. The reason for this is that only few decay events of cluster emission are detected in experiment [17]. Nevertheless, one can see that the calculated half-lives of various cluster emissions are in good agreement with the available experimental data. The standard deviations are $\sigma_{e-e} = 0.29$ for even-even emitters and $\sigma_{o-A} = 0.42$ for odd-A ones, which correspond to the absolute deviation of half-lives with mean factors of 2.0 and 2.6. As one would expect, the results of odd-A emitters are generally less accurate than those of even-even ones. This is due to the addition complication resulting from unpaired nucleons, such as the uncertainty of ℓ values and the fine structure in the cluster energy spectrum. The analytical formula of half-lives

TABLE I. Comparison of the calculated half-lives with the experimental data for emissions of various clusters. Calculations are performed in two ways: by working in the framework of the generalized density-dependent cluster model (GDDCM) and by using the unified formula Eq. (16). The decay Q values and calculated P_c values are presented as well.

Decay	Q (MeV)	P_c	$\log_{10} T_{1/2}^{\text{expt}}$ (s)	$\log_{10} T_{1/2}^{\text{calc}}$ (s)	$\log_{10} T_{1/2}^{\text{formula}}$ (s)
$^{210}\text{Pb} \rightarrow {}^{206}\text{Hg} + {}^{4}\text{He}$	3.792	2.40×10^{-1}	16.57	16.51	15.28
$^{211}\text{Bi} \rightarrow {}^{207}\text{Tl} + {}^{4}\text{He}$	6.751	1.21×10^{-2}	2.18	2.41	1.10
$^{211}\text{Po} \rightarrow {}^{207}\text{Pb} + {}^{4}\text{He}$	7.594	1.19×10^{-2}	−0.28	−0.08	−1.30
$^{212}\text{Po} \rightarrow {}^{208}\text{Pb} + {}^{4}\text{He}$	8.954	2.31×10^{-1}	−6.52	−6.55	−6.49
$^{214}\text{Po} \rightarrow {}^{210}\text{Pb} + {}^{4}\text{He}$	7.833	2.31×10^{-1}	−3.78	−3.55	−3.52
$^{221}\text{Fr} \rightarrow {}^{207}\text{Tl} + {}^{14}\text{C}$	31.29	1.69×10^{-5}	14.56	15.00	15.27
$^{221}\text{Ra} \rightarrow {}^{207}\text{Pb} + {}^{14}\text{C}$	32.40	1.59×10^{-5}	13.39	13.88	14.09
$^{222}\text{Ra} \rightarrow {}^{208}\text{Pb} + {}^{14}\text{C}$	33.05	3.11×10^{-4}	11.22	11.07	11.35
$^{223}\text{Ra} \rightarrow {}^{209}\text{Pb} + {}^{14}\text{C}$	31.83	1.59×10^{-5}	15.05	14.88	15.19
$^{224}\text{Ra} \rightarrow {}^{210}\text{Pb} + {}^{14}\text{C}$	30.54	3.10×10^{-4}	15.87	15.89	16.31
$^{226}\text{Ra} \rightarrow {}^{212}\text{Pb} + {}^{14}\text{C}$	28.20	3.09×10^{-4}	21.20	21.01	21.50
$^{228}\text{Th} \rightarrow {}^{208}\text{Pb} + {}^{20}\text{O}$	44.72	9.40×10^{-6}	20.73	21.24	21.80
$^{230}\text{Th} \rightarrow {}^{206}\text{Hg} + {}^{24}\text{Ne}$	57.76	6.88×10^{-7}	24.63	24.74	24.66
$^{231}\text{Pa} \rightarrow {}^{208}\text{Pb} + {}^{23}\text{F}$	51.84	8.70×10^{-8}	26.02	25.24	26.09
$^{231}\text{Pa} \rightarrow {}^{207}\text{Tl} + {}^{24}\text{Ne}$	60.41	3.18×10^{-8}	22.89	23.24	23.34
$^{232}\text{U} \rightarrow {}^{208}\text{Pb} + {}^{24}\text{Ne}$	62.31	5.61×10^{-7}	20.39	20.37	20.32
$^{233}\text{U} \rightarrow {}^{209}\text{Pb} + {}^{24}\text{Ne}$	60.49	2.86×10^{-8}	24.84	24.43	24.69
$^{233}\text{U} \rightarrow {}^{208}\text{Pb} + {}^{25}\text{Ne}$	60.78	2.14×10^{-8}	24.84	24.48	25.02
$^{234}\text{U} \rightarrow {}^{210}\text{Pb} + {}^{24}\text{Ne}$	58.83	5.57×10^{-7}	25.93	25.64	25.90
$^{234}\text{U} \rightarrow {}^{208}\text{Pb} + {}^{26}\text{Ne}$	59.47	3.14×10^{-7}	25.93	25.66	26.49
$^{234}\text{U} \rightarrow {}^{206}\text{Hg} + {}^{28}\text{Mg}$	74.11	4.48×10^{-8}	25.53	25.57	25.10
$^{236}\text{Pu} \rightarrow {}^{208}\text{Pb} + {}^{28}\text{Mg}$	79.67	3.53×10^{-8}	21.52	21.01	20.48
$^{238}\text{Pu} \rightarrow {}^{210}\text{Pb} + {}^{28}\text{Mg}$	75.91	3.49×10^{-8}	25.70	25.95	25.80
$^{238}\text{Pu} \rightarrow {}^{208}\text{Pb} + {}^{30}\text{Mg}$	76.82	1.98×10^{-8}	25.70	25.43	25.85
$^{238}\text{Pu} \rightarrow {}^{206}\text{Hg} + {}^{32}\text{Si}$	91.19	3.07×10^{-9}	25.28	25.98	25.19
$^{242}\text{Cm} \rightarrow {}^{208}\text{Pb} + {}^{34}\text{Si}$	96.51	1.32×10^{-9}	23.15	23.06	23.00

also gives a precise description of various cluster emissions, although the agreement between experiment and theory is not as good as that of the GDDCM. In addition, we compare the calculated P_c values for even-even emitters with the ones for odd-A emitters. It is found that for a given radioactivity the P_c factors in odd-A emitters are smaller by one order of magnitude than in neighboring even-even emitters. This can easily be explained if the decays of odd-A emitters are hindered by some structure effects. Indeed, the ground states of an odd-A parent nucleus and its daughter generally differ in their structure, which leads to an additional hindrance to the transition between these two states. Furthermore, the present results of P_c agree well with the previous analysis of the odd-A ^{14}C emitters [44], where the ^{14}C radioactivity of two exotic odd-A emitters ^{221}Fr and ^{221}Ra seems to exhibit a one-order-of-magnitude hindrance with respect to the one of neighboring even-even emitters.

Figure 5 shows the deviations of calculated cluster-emission half-lives from the experimental data as a function of the parent nucleus. As one can see, the values of $\log_{10}(T_{\text{calc}}/T_{\text{expt}})$ are generally within the range of ± 0.7, which corresponds to the deviation of half-lives within a factor of 5.0. This means that the calculated half-lives are in good agreement with the experimental data for both even-even and odd-A nuclei. One can also notice that there is a slightly large derivation in Fig. 5, which corresponds to the ^{23}F emitter ^{231}Pa. The emission of ^{23}F from ^{231}Pa is the first example of emissions of an odd-Z cluster in exotic cluster radioactivity. The large

TABLE II. Special cases of the cluster emission of odd-A nuclei, where the exotic cluster emissions do not seem to exhibit any special hindrance, behaving as emissions of even-even emitters. The P_c values, extracted from the experimental data, are apparently larger than the calculated ones for odd-A emitters but comparable with the calculated ones for even-even emitters, clearly showing this rather interesting phenomenon.

Decay	Q (MeV)	$\log_{10} T_{1/2}^{\text{expt}}$ (s)	P_c^{expt}	$P_{c,o-A}^{\text{calc}}$	$P_{c,e-e}^{\text{calc}}$
$^{213}\text{Po} \rightarrow {}^{209}\text{Pb} + {}^{4}\text{He}$	8.536	−5.38	1.71×10^{-1}	1.19×10^{-2}	2.31×10^{-1}
$^{223}\text{Ac} \rightarrow {}^{209}\text{Bi} + {}^{14}\text{C}$	33.06	12.60	8.88×10^{-5}	1.50×10^{-5}	2.93×10^{-4}
$^{225}\text{Ac} \rightarrow {}^{211}\text{Bi} + {}^{14}\text{C}$	30.48	17.28	3.03×10^{-4}	1.49×10^{-5}	2.92×10^{-4}

TABLE III. Predicted half-lives for possible cluster emissions by the GDDCM and by the unified formula Eq. (16). The calculated cluster preformation factors are also listed.

Decay	Q (MeV)	P_c	$\log_{10} T_{1/2}^{\text{expt}}$ (s)	$\log_{10} T_{1/2}^{\text{calc}}$ (s)	$\log_{10} T_{1/2}^{\text{formula}}$ (s)
$^{219}\text{Rn} \rightarrow {}^{205}\text{Hg} + {}^{14}\text{C}$	28.10	1.80×10^{-5}	–	21.06	21.07
$^{220}\text{Rn} \rightarrow {}^{206}\text{Hg} + {}^{14}\text{C}$	28.54	3.51×10^{-4}	–	18.44	18.56
$^{221}\text{Fr} \rightarrow {}^{206}\text{Hg} + {}^{15}\text{N}$	34.12	5.97×10^{-6}	–	23.10	22.88
$^{223}\text{Ra} \rightarrow {}^{205}\text{Hg} + {}^{18}\text{O}$	40.30	1.05×10^{-6}	–	27.28	27.07
$^{225}\text{Ra} \rightarrow {}^{211}\text{Pb} + {}^{14}\text{C}$	29.47	1.58×10^{-5}	–	19.70	20.12
$^{225}\text{Ra} \rightarrow {}^{205}\text{Hg} + {}^{20}\text{O}$	40.48	5.71×10^{-7}	–	28.55	28.99
$^{226}\text{Ra} \rightarrow {}^{206}\text{Hg} + {}^{20}\text{O}$	40.82	1.11×10^{-5}	–	26.37	26.80
$^{223}\text{Ac} \rightarrow {}^{208}\text{Pb} + {}^{15}\text{N}$	39.47	5.21×10^{-6}	>14.76	15.06	14.99
$^{227}\text{Ac} \rightarrow {}^{207}\text{Tl} + {}^{20}\text{O}$	43.09	5.23×10^{-7}	–	24.43	25.10
$^{229}\text{Ac} \rightarrow {}^{206}\text{Hg} + {}^{23}\text{F}$	48.36	1.05×10^{-7}	–	28.73	29.62
$^{226}\text{Th} \rightarrow {}^{208}\text{Pb} + {}^{18}\text{O}$	45.73	1.75×10^{-5}	>16.76	18.14	18.04
$^{226}\text{Th} \rightarrow {}^{212}\text{Po} + {}^{14}\text{C}$	30.55	2.75×10^{-4}	>15.30	17.92	18.31
$^{227}\text{Th} \rightarrow {}^{209}\text{Pb} + {}^{18}\text{O}$	44.20	8.94×10^{-7}	–	22.22	22.23
$^{228}\text{Th} \rightarrow {}^{206}\text{Hg} + {}^{22}\text{Ne}$	55.74	1.26×10^{-6}	–	26.94	26.24
$^{229}\text{Th} \rightarrow {}^{209}\text{Pb} + {}^{20}\text{O}$	43.40	4.80×10^{-7}	–	25.02	25.81
$^{229}\text{Th} \rightarrow {}^{205}\text{Hg} + {}^{24}\text{Ne}$	57.83	3.54×10^{-8}	–	26.21	26.05
$^{231}\text{Th} \rightarrow {}^{207}\text{Hg} + {}^{24}\text{Ne}$	55.99	3.51×10^{-8}	–	29.01	29.22
$^{231}\text{Th} \rightarrow {}^{206}\text{Hg} + {}^{25}\text{Ne}$	56.87	2.64×10^{-8}	–	28.07	28.54
$^{232}\text{Th} \rightarrow {}^{208}\text{Hg} + {}^{24}\text{Ne}$	54.42	6.83×10^{-7}	>29.20	30.34	30.53
$^{232}\text{Th} \rightarrow {}^{206}\text{Hg} + {}^{26}\text{Ne}$	55.96	3.88×10^{-7}	>29.20	28.77	29.50
$^{227}\text{Pa} \rightarrow {}^{209}\text{Bi} + {}^{18}\text{O}$	45.87	8.28×10^{-7}	–	20.46	20.50
$^{229}\text{Pa} \rightarrow {}^{207}\text{Tl} + {}^{22}\text{Ne}$	58.96	5.86×10^{-8}	–	24.37	23.95
$^{230}\text{U} \rightarrow {}^{208}\text{Pb} + {}^{22}\text{Ne}$	61.39	1.04×10^{-6}	>18.20	21.04	20.11
$^{230}\text{U} \rightarrow {}^{206}\text{Pb} + {}^{24}\text{Ne}$	61.35	5.66×10^{-7}	>18.20	22.14	21.78
$^{232}\text{U} \rightarrow {}^{204}\text{Hg} + {}^{28}\text{Mg}$	74.32	4.53×10^{-8}	>22.26	25.64	24.77
$^{233}\text{U} \rightarrow {}^{205}\text{Hg} + {}^{28}\text{Mg}$	74.23	2.31×10^{-9}	>27.59	27.00	26.43
$^{235}\text{U} \rightarrow {}^{211}\text{Pb} + {}^{24}\text{Ne}$	57.36	2.84×10^{-8}	>27.65	29.22	29.91
$^{235}\text{U} \rightarrow {}^{210}\text{Pb} + {}^{25}\text{Ne}$	57.76	2.12×10^{-8}	>27.65	29.22	30.12
$^{235}\text{U} \rightarrow {}^{207}\text{Hg} + {}^{28}\text{Mg}$	72.16	2.28×10^{-9}	>28.45	29.56	29.57
$^{235}\text{U} \rightarrow {}^{206}\text{Hg} + {}^{29}\text{Mg}$	72.49	1.72×10^{-9}	>28.45	29.57	29.80
$^{236}\text{U} \rightarrow {}^{212}\text{Pb} + {}^{24}\text{Ne}$	55.95	5.52×10^{-7}	>26.27	30.41	30.92
$^{236}\text{U} \rightarrow {}^{210}\text{Pb} + {}^{26}\text{Ne}$	56.75	3.11×10^{-7}	>26.27	30.21	31.30
$^{236}\text{U} \rightarrow {}^{208}\text{Hg} + {}^{28}\text{Mg}$	70.48	4.44×10^{-8}	>26.27	30.83	30.69
$^{236}\text{U} \rightarrow {}^{206}\text{Hg} + {}^{30}\text{Mg}$	72.51	2.54×10^{-8}	>26.27	28.91	29.32
$^{238}\text{U} \rightarrow {}^{208}\text{Hg} + {}^{30}\text{Mg}$	69.24	2.51×10^{-8}	–	33.63	34.35
$^{231}\text{Np} \rightarrow {}^{209}\text{Bi} + {}^{22}\text{Ne}$	61.91	4.82×10^{-8}	–	22.76	22.22
$^{233}\text{Np} \rightarrow {}^{209}\text{Bi} + {}^{24}\text{Ne}$	62.16	2.60×10^{-8}	–	23.28	23.49
$^{235}\text{Np} \rightarrow {}^{207}\text{Tl} + {}^{28}\text{Mg}$	77.10	2.04×10^{-9}	–	24.19	23.95
$^{237}\text{Np} \rightarrow {}^{207}\text{Tl} + {}^{30}\text{Mg}$	74.82	1.15×10^{-9}	>27.57	28.01	28.67
$^{237}\text{Pu} \rightarrow {}^{209}\text{Pb} + {}^{28}\text{Mg}$	77.73	1.80×10^{-9}	–	24.73	24.69
$^{237}\text{Pu} \rightarrow {}^{208}\text{Pb} + {}^{29}\text{Mg}$	77.46	1.35×10^{-9}	–	25.52	25.74
$^{237}\text{Pu} \rightarrow {}^{205}\text{Hg} + {}^{32}\text{Si}$	91.46	1.58×10^{-10}	–	27.14	26.32
$^{239}\text{Pu} \rightarrow {}^{209}\text{Pb} + {}^{30}\text{Mg}$	75.12	1.01×10^{-9}	–	29.28	29.94
$^{239}\text{Pu} \rightarrow {}^{205}\text{Hg} + {}^{34}\text{Si}$	91.86	9.03×10^{-11}	–	27.07	26.99
$^{237}\text{Am} \rightarrow {}^{209}\text{Bi} + {}^{28}\text{Mg}$	79.90	1.60×10^{-9}	–	23.63	23.26
$^{239}\text{Am} \rightarrow {}^{207}\text{Tl} + {}^{32}\text{Si}$	94.51	1.37×10^{-10}	–	24.91	24.15
$^{241}\text{Am} \rightarrow {}^{207}\text{Tl} + {}^{34}\text{Si}$	93.93	7.77×10^{-11}	>24.41	26.00	26.08
$^{240}\text{Cm} \rightarrow {}^{208}\text{Pb} + {}^{32}\text{Si}$	97.56	2.32×10^{-9}	–	21.48	20.56
$^{241}\text{Cm} \rightarrow {}^{209}\text{Pb} + {}^{32}\text{Si}$	95.40	1.18×10^{-10}	–	25.42	24.80
$^{243}\text{Cm} \rightarrow {}^{209}\text{Pb} + {}^{34}\text{Si}$	94.75	6.69×10^{-11}	–	26.53	26.83
$^{244}\text{Cm} \rightarrow {}^{210}\text{Pb} + {}^{34}\text{Si}$	93.14	1.30×10^{-9}	–	27.15	27.51

deviation of its half-lives can be understood as being the difference between the emissions of an odd-Z cluster and of an even-Z cluster. It should be noted that another new emission of an odd-Z cluster, namely the ^{15}N emission from ^{223}Ac [18], has recently been observed, together with a low limit of its half-life. Along with the accumulation of data on emissions of odd-Z clusters, it would be very interesting to investigate the even-odd effect of the proton number for various clusters.

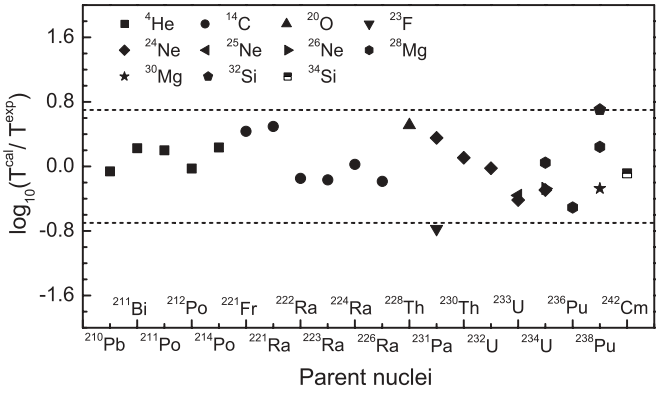

FIG. 5. Deviation of cluster emission half-lives calculated within the GDDCM framework from the experimental data for various clusters. Different parent nuclei are indicated at the bottom.

Before we finish the discussion of the numerical results, we would like to point out some special cases of the cluster emission of odd-A nuclei. As already mentioned, the radioactivity of odd-A emitters in most cases exhibits strong hindrance. However, some special cases seem to exhibit no hindrance just like the decay of even-even emitters. The representative example is the α decay of ^{213}Po from the ground state with the $9/2^{+}$ spin-parity to the daughter ground state with the same spin-parity [45]. It involves only the paired nucleons forming an α cluster, which is strikingly different from the hindered α decays of ^{211}Bi and ^{211}Po that involve the unpaired nucleons and the proton- or neutron-shell crossing. In exotic cluster radioactivity, it is known that the centrifugal barrier has a rather weak effect on the decay widths, as shown in Fig. 3. Therefore, without consideration of the exact ℓ values, one can pick up the unhindered cluster emissions of odd-A emitters by comparing the experimental P_c values with the calculated ones. They are listed in Table II, together with the α decay of ^{213}Po. The fourth column of Table II denotes the experimental P_c value, which is extracted from the experimental half-life. The last two columns denote the calculated P_c values in two groups of odd-A and even-even emitters. Obviously, the experimental P_c values are significantly larger than the calculated ones for odd-A emitters but comparable with the calculated ones for even-even emitters. This demonstrates that the cluster emissions of the odd-A emitters shown in Table II indeed belong to the unhindered decays, behaving as one of the even-even emitters. For the ^{14}C emission of ^{225}Ac, the tentative interpretation of the unhindered ground-state-to-ground-state transition was given in Ref. [46], that is, the deformed $3/2^{-}$ configuration, assigned to the ^{225}Ac ground state, originates from the unperturbed spherical $9/2^{-}$ state which serves as the ground state of the daughter nucleus ^{211}Bi. The theoretical calculation of the ^{225}Ac structure also provided the other possible situation that the unhindered decay could occur for the transition to the first excited $7/2^{-}$ state of the daughter nucleus ^{211}Bi. Motivated by the nuclear structure arguments in ^{225}Ac, the experiment on the radioactivity of ^{233}Ac was achieved, where the ^{14}C emission was found to be as unhindered as emissions of even-even emitters and interpreted as the ground-state-to-ground-state transition in terms of the ^{223}Ac ground-state configuration.

The good agreement between experiments and calculations shown in Table I and Fig. 5 confirms the applicability and validity of the GDDCM for cluster radioactivity and allows us to make reliable predictions of half-lives for emissions of known clusters from promising candidates. In Table III, we present the detailed predictions of cluster emission half-lives by working in the framework of the GDDCM and by using the unified formula Eq. (16). The calculated P_c values are also given. It will be of significant interest to compare the present theoretical predictions with future experimental observations.

IV. SUMMARY

In summary, we have presented in this paper an extension of the newly developed GDDCM to study cluster radioactivity. In the GDDCM, the microscopic cluster-daughter potential is numerically constructed in the double-folding model for both Coulomb and nuclear parts. Instead of working in the WKB framework, the exact solution of the Schrödinger equation with outgoing Coulomb wave boundary conditions is presented for the calculation of the decay width. Based on some available experimental cases, the cluster preformation factor is evaluated by the simple analytical formula. The results reported in Table I are in good agreement with the available experimental data, and some useful predictions of half-lives are made for emissions of known clusters from possible candidates. Despite this, the preset analysis is merely the beginning because many open problems are still unsolvable, such as the even-odd effect of proton number for various clusters, the fine structure in the cluster energy spectrum, the possible cluster emissions in the trans-tin region, the wide variation of nuclear deformation from a parent nucleus to its daughter, and the microscopic interpretation of cluster preformation. Efforts toward the complete understanding of cluster radioactivity are being made from both experimental and theoretical sides.

ACKNOWLEDGMENTS

This work is supported by the National Natural Science Foundation of China (Grants Nos. 10535010, 10675090, 10775068, 10735010, and 10975072), by the 973 National Major State Basic Research and Development of China (Grants Nos. 2007CB815004 and 2010CB327803), by CAS Knowledge Innovation Project No. KJCX2-SW-N02, and by Research Fund of Doctoral Point (RFDP), Grant No. 20070284016.

[1] A. Săndulescu, D. N. Poenaru, and W. Greiner, Sov. J. Part. Nucl. **11**, 528 (1980).
[2] H. J. Rose and G. A. Jones, Nature (London) **307**, 245 (1984).
[3] D. N. Poenaru, M. Ivaşcu, A. Sandulescu, and W. Greiner, Phys. Rev. C **32**, 572 (1985).
[4] W. Greiner, M. Ivaşcu, D. N. Poenaru, and A. Sandulescu, Z. Phys. A **320**, 347 (1985).

[5] Yi-Jin Shi and W. J. Swiatecki, Phys. Rev. Lett. **54**, 300 (1985).
[6] D. N. Poenaru and W. Greiner, Phys. Scr. **44**, 427 (1991).
[7] G. Royer and R. Moustabchir, Nucl. Phys. A **683**, 182 (2001).
[8] K. P. Santhosh, R. K. Biju, and S. Sahadevan, Nucl. Phys. A **838**, 38 (2010).
[9] S. S. Malik and R. K. Gupta, Phys. Rev. C **39**, 1992 (1989).
[10] B. Buck and A. C. Merchant, Phys. Rev. C **39**, 2097 (1989).
[11] R. G. Lovas, R. J. Liotta, A. Insolia, K. Varga, and D. S. Delion, Phys. Rep. **294**, 265 (1998).
[12] S. K. Arun, R. K. Gupta, B. B. Singh, S. Kanwar, and M. K. Sharma, Phys. Rev. C **79**, 064616 (2009); S. K. Arun, R. K. Gupta, S. Kanwar, B. B. Singh, and M. K. Sharma, *ibid.* **80**, 034317 (2009).
[13] Zhongzhou Ren, Chang Xu, and Zaijun Wang, Phys. Rev. C **70**, 034304 (2004).
[14] S. N. Kuklin, G. G. Adamian, and N. V. Antonenko, Phys. Rev. C **71**, 014301 (2005).
[15] F. R. Xu and J. C. Pei, Phys. Lett. B **642**, 322 (2006).
[16] H. F. Zhang, J. M. Dong, G. Royer, W. Zuo, and J. Q. Li, Phys. Rev. C **80**, 037307 (2009).
[17] R. Bonetti and A. Guglielmetti, Romanian Rep. Phys. **59**, 301 (2007).
[18] A. Guglielmetti *et al.*, J. Phys.: Conf. Ser. **111**, 012050 (2008).
[19] D. N. Poenaru, I.-H. Plonski, and W. Greiner, Phys. Rev. C **74**, 014312 (2006).
[20] K. P. Santhosh, R. K. Biju, and Antony Joseph, J. Phys. G **35**, 085102 (2008).
[21] Dongdong Ni, Zhongzhou Ren, Tiekuang Dong, and Chang Xu, Phys. Rev. C **78**, 044310 (2008).
[22] D. S. Delion, Phys. Rev. C **80**, 024310 (2009).
[23] D. N. Poenaru, R. A. Gherghescu, and W. Greiner, J. Phys. G: Nucl. Part. Phys. **36**, 125101 (2009).
[24] D. N. Poenaru and W. Greiner, Nucl. Phys. A **834**, 163c (2010).
[25] Dongdong Ni and Zhongzhou Ren, Phys. Rev. C **80**, 014314 (2009).
[26] Dongdong Ni and Zhongzhou Ren, J. Phys. G **37**, 035104 (2010).
[27] Dongdong Ni and Zhongzhou Ren, Phys. Rev. C **80**, 051303(R) (2009); **81**, 024315 (2010).
[28] V. Yu. Denisov and H. Ikezoe, Phys. Rev. C **72**, 064613 (2005).
[29] P. Mohr, Phys. Rev. C **73**, 031301(R) (2006).
[30] N. G. Kelkar and H. M. Castañeda, Phys. Rev. C **76**, 064605 (2007).
[31] G. Bertsch, J. Borysowicz, H. Mcmanus, and W. G. Love, Nucl. Phys. A **284**, 399 (1977).
[32] A. M. Kobos, B. A. Brown, P. E. Hodgson, G. R. Satchler, and A. Budzanowski, Nucl. Phys. A **384**, 65 (1982).
[33] Chang Xu and Zhongzhou Ren, Phys. Rev. C **73**, 041301(R) (2006); **74**, 014304 (2006).
[34] M. A. Preston and R. K. Bhaduri, *Structure of the Nucleus* (Addison-Wesley, Reading, MA, 1975).
[35] J. D. Walecka, *Theoretical Nuclear Physics and Subnuclear Physics* (Oxford University, Oxford, 1995).
[36] G. R. Satchler and W. G. Love, Phys. Rep. **55**, 183 (1979).
[37] K. Wildermuth and Y. C. Tang, *A Unified Theory of the Nucleus* (Academic, New York, 1997).
[38] H. Horiuchi, J. Phys. G **37**, 064021 (2010).
[39] M. Iriondo, D. Jerrestam, and R. J. Liotta, Nucl. Phys. A **454**, 252 (1986).
[40] P. E. Hodgson and E. Běták, Phys. Rep. **374**, 1 (2003).
[41] R. Blendowske and H. Walliser, Phys. Rev. Lett. **61**, 1930 (1988).
[42] K. Varga, R. G. Lovas, and R. J. Liotta, Phys. Rev. Lett. **69**, 37 (1992).
[43] G. Audi, A. H. Wapstra, and C. Thibault, Nucl. Phys. A **729**, 337 (2003).
[44] R. Bonetti *et al.*, Nucl. Phys. A **576**, 21 (1994).
[45] R. B. Firestone, V. S. Shirley, C. M. Baglin, S. Y. Frank Chu, and J. Zipkin, *Table of Isotopes*, 8th ed. (Wiley Intersicence, New York, 1996).
[46] R. Bonetti *et al.*, Nucl. Phys. A **562**, 32 (1993).